Contrib Mineral Petrol (2000) 140: 40–54

Raffaello Cioni

Volatile content and degassing processes in the AD 79 magma chamber at Vesuvius (Italy)

Received: 28 October 1999 / Accepted: 21 April 2000

Abstract The evolution of volatiles in the AD 79 magma chamber at Vesuvius (Italy) was investigated through the study of melt inclusions (MI) in crystals of different origins. FTIR spectroscopy and EMPA were used to measure H_2O, CO_2, S and Cl of the different melts. This allowed us to define the volatile content of the most evolved, phonolitic portion of the magma chamber and of the mafic melts feeding the chamber. MI in sanidine from phonolitic and tephri-phonolitic pumices show systematic differences in composition and volatile content, which can be explained by resorption of the host mineral during syn-eruptive mixing. The pre-eruption content of phonolitic magma appears to have been dominated by H_2O and Cl (respectively 6.0 to 6.5 wt% and 6700 ppm), while magma chamber refilling occurred through the repeated injection of H_2O, CO_2 and S-rich tephritic magmas (respectively 3%, 1500 ppm and 1400 ppm). Strong CO_2 degassing probably occurred during the decompressional path of mafic batches towards the magma chamber, while sulphur was probably released by the magma following crystallization and mixing processes. Water and chlorine strongly accumulated in the magma and reached their solubility limits only during the eruption. Chlorine solubility appears to have been strongly compositionally controlled, and Cl release was inhibited by groundmass crystallization of leucite, which shifted the composition of the residual liquid towards higher Cl solubilities.

R. Cioni
Dipartimento di Scienze della Terra, V.S. Maria 53,
56126 Pisa, Italy
e-mail: rcioni@unica.it

Present address:
R. Cioni, Dipartimento di Scienze della Terra,
Via Trentino 51, 09127 Cagliari, Italy

Editorial responsibility: T. L. Grove

Introduction

Magma chamber evolution and eruptive processes are strongly influenced by magmatic volatiles. Their effects are especially important in large silicic magma chambers, where volatiles can reach high concentrations. Closed-system exsolution of volatiles (especially water) from magma leads to the formation of large eruptive columns (Wilson et al. 1980; Sparks 1986) and to the almost complete evacuation of magma chambers, with dramatic effects on the geometry of the magmatic systems. In addition, dissolved magmatic volatiles and coexisting fluid phases strongly control the evolution of silicate melts, determining liquidus temperature and mineral assemblages.

The presence of different volatile species in a magma modifies the saturation value of each species at a given pressure (Holloway and Blank 1994; Dixon and Stolper 1995; Papale 1997; Webster 1997), and a comprehensive study of the main volatile components (H_2O, CO_2, Cl, F, S) should always be carried out in order to describe the main features of a pre-eruptive silicate melt.

Pre-eruptive melts are sometimes preserved in glassy, not crystallized melt inclusions (MI) in minerals (Johnson et al. 1994; Lowenstern 1994a), and composition and temperature of these inclusions can give insights into the liquid line of descent of the magma. Information on the composition and amount of the syn-eruptively released fluid phase derives from comparison with the volatile content in the groundmass of erupted products (Barclay et al. 1996).

This paper is mainly aimed at defining the pre-eruption conditions of the AD 79 Vesuvius magma chamber through the study of the composition and volatile content of MI from different mineral phases (with the assumption that they represent the pre-entrapment magma composition). The data allow us to make inferences regarding the mechanism of volatile accumulation and degassing in the different portions of the magma

chamber, and to draw some general conclusions about the behaviour of the volatile component in these K-phonolitic magmas.

Geological framework

On 24 August AD 79, Vesuvius awoke after some hundreds of years of inactivity. The products of the eruption buried the Roman towns of Pompeii, Herculaneum and Stabiae, and the surrounding plain. The eruption progressed from a weak, phreatomagmatic opening phase, to a climactic Plinian phase, and to a final phreatomagmatic phase, triggered by the collapse of the caldera (Sigurdsson et al. 1985; Cioni et al. 1992). The deposits of the eruption are summarized in Fig. 1, together with a brief description of the main phases of the eruption. About 80% of the total magma volume was erupted during the Plinian phase, and dispersed as a widespread pumice fall blanket only interrupted, in the more proximal sites, by some minor deposits of pyroclastic density currents. The fall deposit is characterized by a sharp colour and compositional zoning, from white phonolitic to grey tephri-phonolitic pumice. The final phreatomagmatic phase is mainly represented by pyroclastic flow and surge deposits whose sedimentological features reveal a progressive increase of the presence of external water in the pyroclastic clouds.

The geochemical and petrographic features of the erupted products were studied in detail by Sigurdsson et al. (1990), Mues-Schumacher (1994) and Cioni et al. (1995). White phonolitic and grey tephri-phonolitic pumice have a mineral assemblage consisting of sanidine, diopsidic pyroxene, salitic pyroxene, phlogopite, K-ferripargasitic amphibole and melanitic garnet, the main difference being the modal proportions of each phase. Leucite is very abundant in the groundmass, and quite rare as a phenocryst.

Important syn-eruptive mixing processes govern the composition of the erupted magma, as revealed by mineral chemistry, MI composition and isotopic features of whole rock and mineral phases (Cioni et al. 1995). All the products can be described as the result of a mixing between three end members: a salic end member with the composition of the first erupted white phonolitic pumice, a cumulitic end member supplying mafic crystals to the mineral assemblage of the erupted products, and a mafic end member, never erupted without being mixed, whose composition can be calculated on the basis of the mineral assemblage of the pumice. MI in sanidine, amphibole, garnet and salitic pyroxene have compositions similar to the salic end member, while inclusions in diopside have tephritic to basanitic compositions. Cioni et al. (1995) and Marianelli et al. (1995) related these compositions to mafic magma batches periodically

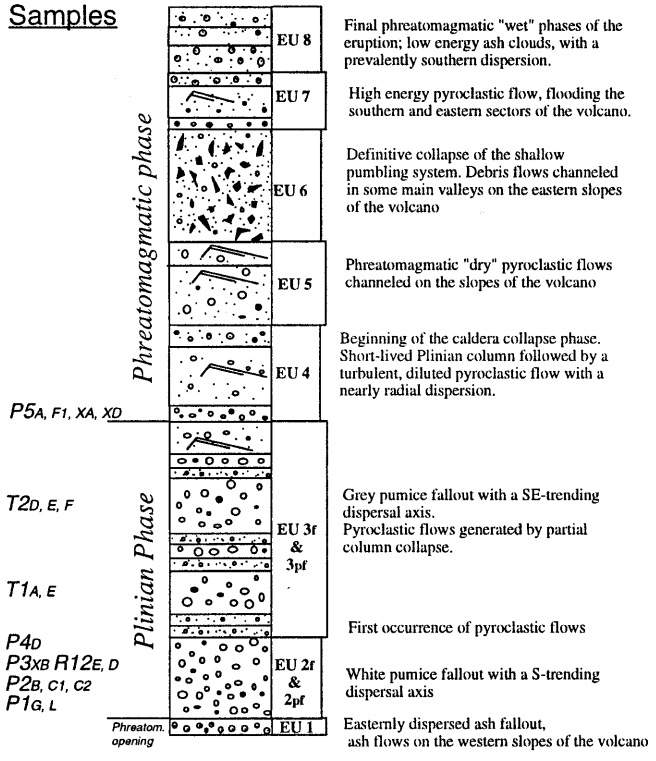

Fig. 1 General stratigraphy of the AD 79 eruption and sampling localities. The samples are placed at the equivalent stratigraphic height. Samples T1A,E and T2D,E,F are from Tricino site; samples R12E,D are from Oplontis excavations; samples P1G,L, P2B,C1,C2, P3XB, P4D and P5A,F1,XA,XD are from Pozzelle quarry

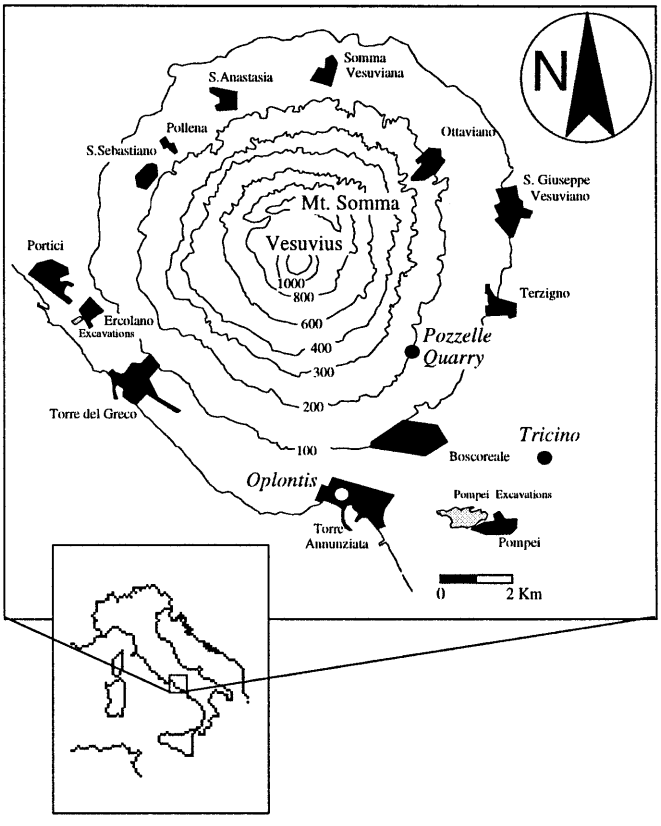

feeding a growing and differentiating chamber. In this view, the mafic end member could represent a magma body which acted as a compositional and thermal buffer to the discrete arrivals of the hot, tephritic batches. The absence of crystals in equilibrium with the mafic end member suggests that it could have been in a slightly superheated state.

Sampling and sample preparation

In this study, MI in sanidine, leucite and diopside from different phases of the eruption were analysed. More than 2 kg of coarse pumice lapilli were sampled at different stratigraphic heights in the fall and flow deposits, both from the Plinian and the final phreatomagmatic phases (Fig. 1). Studied pumices were sampled at two different locations, respectively 5 km (Pozzelle Quarry, Fig. 1) and 8 km (Tricino, Fig. 1) southeast of the present Vesuvius crater. After washing, the pumices were crushed in a steel mortar and then sieved. The procedure was repeated for fragments larger than 4 mm in diameter, in order to obtain a greater number of 2, 1 and 0.5 mm fragments. Crystals were then separated from these three grain sizes by water panning followed by hand-picking. For each sample, more than 20 crystals of mafic and salic minerals were selected on the basis of the presence of MI, after microscopic viewing with immersion oil. The selected crystals were then embedded in orthodontic resin and polished on one side with alumina papers and powder (down to 0.25 μm) to expose the MI. For the salic minerals (mainly sanidine and minor leucite), only those crystals with homogeneous, not crystallized glassy inclusions were chosen for the double polishing. These crystals were glued to a glass slide with a plastic cement (Crystal Bond, Aremco) and polished on the other side. Crystals were then removed from the glass slides and rinsed in acetone and ethanol. Thickness was measured with an electronic micrometer (Mitutoyo Digimatic Indicator), with a precision of ±1 μm. For each crystal, three measurements were made as close as possible to the MI, and the arithmetic mean was chosen. Due to the size of the MI in sanidine, the final thickness was often thinner than 20 μm. In such cases, host crystals were often strongly fractured by the polishing procedure, and their removal from the slide was very difficult. Before removal, we performed FTIR spectra on these "high risk" inclusions, to have additional information to use in the case of damage to samples during removal from the slide. In fact, some doubly polished inclusions were lost while being removed from the glass slide.

Due to the opaque, microcrystalline aspect of MI in pyroxene, diopside crystals were heated before polishing in a furnace with a controlled atmosphere (QFM buffer), at 1200 °C for 15 min. The temperature and duration of heating was determined on the basis of the MI homogenization kinetics of Marianelli et al. (1995). Only a few large inclusions did not decrepitate. Four of these were selected for double polishing and FTIR measurements.

Analytical methods

Electron probe

The composition of MI and host minerals was determined by EPMA analyses with a Jeol SuperProbe JX4-8600 equipped with a Tracor Northern WDS system (at Centro per la Minerogenesi dell'Appennino, CNR, Florence). Analyses were performed with an acceleration voltage of 15 kV and a beam current of 10 nA. To prevent Na loss glasses were analysed using a defocused beam of 10 μm and with a dwell time for Na of 10 s. Dwell time for Ba, Sr, Cl, F and S was 40 s. Three to five analyses were performed on each MI, depending on its size. The composition of the host mineral was measured close to the MI, far enough to avoid the diffusion layer.

Infrared spectroscopy

Phonolitic MI hosted in sanidine and leucite, and tephritic MI in diopsidic pyroxene were analysed by FTIR microspectroscopy to obtain dissolved water and carbon dioxide contents. The measurements were performed in the laboratories of GPS-California Institute of Technology, Pasadena (CA), using a Nicolet 60SX Fourier Transform spectrometer equipped with an MCT detector, a Globar source, a KBr beamsplitter and a NicPlan microscope. Spectra were taken with a resolution of 8 cm^{-1} and a number of scans variable between 1024 and 4096.

Absorbancies were measured from peak heights, after subtraction of the background signal, normally extrapolated with a flexible drawing curve. The concentration of the absorbing species was calculated using the Beer–Lambert law:

$$c_i = 100 \times (MW_i A)/(d\rho^x \varepsilon_i^x)$$

where c_i = species concentration, in wt%; MW_i = molecular weight of the i-th species; A = absorbance, in unit of absorbance; d = sample thickness, in cm; ρ^x = sample density for the x-th glass composition, in g/l; ε_i^x = molar absorptivity of the i-th species for the x-th glass composition, in L/(mol cm).

Density was assumed to vary with glass composition, and was estimated through an iterative method using the Church and Johnson (1980) and Gladstone–Dale rules, as described in Silver et al. (1990).

Three to four spectra were collected on each MI, and the arithmetic mean of the resulting species concentration was calculated.

H_2O^m and OH were recalculated starting from the absorbancies of the 5200 cm^{-1} band (combination stretching and bending mode of molecular water, H_2O^m, groups) and the 4500 cm^{-1} band (combination stretching and bending mode of bounded hydroxyl groups). Experimental values for molar absorptivity (ε) of water in K-phonolitic glasses are at present not available. Carroll and Blank (1997) carried out an experimental study on some Na-phonolites from Tenerife (Canary Islands), concluding that molar absorptivities for water in these composition were similar to those determined for jadeitic glasses by Silver et al. (1990). In particular, the new molar absorptivities ($\varepsilon_{5200} = 1.10^{+0.12}_{-0.10}$ $\varepsilon_{4500} = 1.25^{+0.33}_{-0.22}$) proposed by Carroll and Blank (1997) were statistically indistinguishable from the values for jadeitic melts. The use of experimentally determined values of ε_i on Na-rich instead of K-rich glasses is also in good agreement with the small (not more than 10%) compositional dependence of ε observed by Behrens et al. (1996) between Na and K feldspar glasses. Moreover, Romano et al. (1995), studying $NaAlSi_3O_8$–$KAlSi_3O_8$ melts, concluded that no significant variation in water speciation occurs in the exchange reaction K–Na.

In some samples, due to their small thickness, absolute absorbancies for these two bands were too low and too disturbed by superimposed interference fringes, while good signals came from the bands at 3550 and 1630 cm^{-1}, respectively fundamental OH stretching vibration and fundamental bending mode of water molecules (Stolper 1982). For these two bands, no data were available for molar absorptivities in phonolitic melts, and they were recalculated to best fit the data obtained from the 4500 and 5200 cm^{-1} bands. In particular, Newman et al. (1986), demonstrated that the ratio between the absorbancies per unit thickness of 5200 and 1630 cm^{-1} bands was constant (Fig. 2), and $abs_{5200}/abs_{1630} = \varepsilon_{5200}/\varepsilon_{1630}$.

In our samples, the average value of this ratio was calculated, obtaining a value for ε_{1630} of 32 ± 4, intermediate between the values calculated for rhyolite (55 ± 2; Newman et al. 1986), icelandite (42 ± 2; Jacobsson 1997) and MORB glasses (25 ± 3; Dixon et al. 1995).

The absorptivity of the 3550 cm^{-1} fundamental OH stretching band is dependent on water speciation (equation 2 in Newman et al. 1986). The ratio between OH and H_2O^m varies with the total water content, and values for ε_{3550} must be considered to vary between the values for OH and H_2O^m vibrations for this band. We calculated a mean value of ε_{3550} for the phonolitic compositions, where the total water content (determined from the sum of the

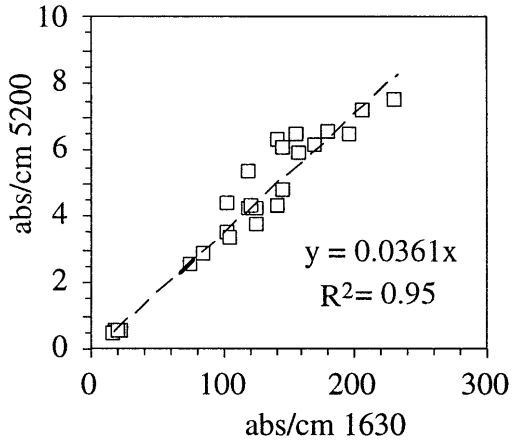

Fig. 2 Linear correlation between absorbancies per unit length of 5200 and 1630 cm^{-1} bands

results from 4500 and 5200 cm^{-1} bands) is always higher than 3–4 wt%. In this case, the mean value for ε_{3550} was 64 ± 8 L/(mol cm). This value is very close to the value of 66 ± 2 L/(mol cm), calculated from OH and H_2O^m assuming molar absorptivities respectively of 88 and 56 L/(mol cm) (Newman et al. 1986; Dobson et al. 1989) for $\varepsilon_{OH,3550}$ and $\varepsilon_{H_2O,3550}$. As a matter of fact, ε_{3550} shows a very low compositional dependence, varying over a quite narrow range (Ihinger et al. 1994).

Values for molar absorptivities in tephritic glasses (MI in diopside) were assumed to be equal to the values for MORB given by Dixon et al. (1995). In particular, we used the values of 25 ± 3 L/(mol cm) for the 1630 cm^{-1} peak, well pronounced in all but one sample, and of 63 ± 5 L/(mol cm) for the 3550 cm^{-1} band. In these MI, the peaks at 4500 and 5200 cm^{-1} are always strongly superimposed by interference fringes, which make interpretation of the spectra difficult.

Carbon dioxide is only present as CO_3^{2-} in the MI in diopside, which gives a doublet absorption band at approximately 1400–1550 cm^{-1}. A mean separation of 80 cm^{-1} was observed on the spectra, in agreement with that observed in ol-nephelinite and phonolite glasses (Blank and Brooker 1994). The molar absorptivity for the related mid-IR bands was calculated on the basis of compositional data according to the best fit proposed by Dixon and Pan (1995), and resulting in $\varepsilon = 380$ L/(mol cm).

A brief summary of the main features of the absorption bands used in this paper is shown in Table 1.

Texture and morphology of melt inclusions

MI of variable size and shape are found in the different mineral phases of the AD 79 magma. Inclusions in sanidine, leucite and pyroxene were chosen for this study and their EPMA compositions are given in Tables 2 to 4. Inclusions in amphibole are generally too small to be prepared and measured by FTIR spectroscopy, while the highly fractured nature of garnet crystals prevented us from obtaining good samples for analysis.

Sanidine

Sanidine was separated from white and grey pumice. It occurs both with the classic flattened habit with prominent (010), and as prisms elongated parallel to the *x*-axis. MI are generally present in those crystals with a flattened habit, which are the most abundant. According to Cioni et al. (1995), the composition of sanidine is quite homogeneous ($Or_{84–87}$; Table 3). Ba and Sr contents are always very low, near the EPMA detection limit (Table 3).

MI are quite rare, and show variable shapes and dimensions. They are generally glassy and light coloured, without any apparent recrystallization or devitrification. Different types of inclusions can be distinguished:

- Rounded to subrounded MI (10 to 70 μm in diameter), often containing several gas bubbles distributed all along the MI–crystal interface (Fig. 3a, b, c).
- Faceted MI, with prismatic shapes and longest dimension up to 80–100 μm. A sanidine rim slightly different in composition sometimes occurs between

Table 2 EPMA compositions of the MI-hosting minerals – leucite

	P5A	P1L	P2C
SiO_2	55.52	55.23	55.50
Al_2O_3	23.10	23.40	23.44
Fe_2O_3	0.22	0.22	0.15
CaO	0	0.02	0.02
Na_2O	0.78	0.96	0.83
K_2O	19.95	19.57	19.39
Si	2.01	2.00	2.01
Al	0.99	1.00	1.00
Fe	0.01	0.01	0
Ca	0	0	0
Na	0.05	0.07	0.06
K	0.92	0.91	0.90
Si + Al	3.00	3.01	3.01
Na + K	0.98	0.98	0.96
Q	0.29	0.29	0.30
Ne	0.04	0.05	0.04
Ks	0.67	0.66	0.66

Table 1 Mean position of the H_2O and CO_2-related infrared peaks in tephritic and phonolitic melts, and values of the corresponding extinction coefficients

	Tephrites		Phonolites	
	Wavenumber (cm^{-1})	ε [L/(mol cm)]	Wavenumber (cm^{-1})	ε [L/(mol cm)]
Fundamental stretching of water molecules	3503 ± 16	63	3469 ± 16	64
Fundamental bending of water molecules	1639 ± 8	25	1637 ± 8	32
Combination stretching and bending of TOH groups	4451 ± 8	0.67	4467 ± 16	1.12
Combination stretching and bending of water molecules	5186 ± 8	0.62	5203 ± 16	1.13
Asymmetric stretching of carbonate molecules	1436 ± 8	380	–	–
Asymmetric stretching of carbonate molecules	1512 ± 8	380	–	–

Table 3 EPMA compositions of the MI-hosting minerals – sanidine

	T1A	T2E	T2D	R12E	T1E	T2F	P5F1	P2B	R12D
SiO_2	63.13	63.56	64.30	64.79	63.82	64.47	64.39	64.00	64.56
Al_2O_3	18.83	19.20	19.41	19.48	19.10	19.80	19.64	19.26	19.00
Fe_2O_3	0.13	0.18	0.12	0.12	0.10	0.08	0.08	0	0.12
CaO	0.28	0.33	0.32	0.21	0.26	0.35	0.45	0.18	0.19
Na_2O	1.38	1.24	1.56	1.51	1.20	1.34	1.24	1.57	1.50
K_2O	14.09	14.74	14.48	13.96	14.40	14.08	14.13	15.00	14.63
Si	2.97	2.95	2.95	2.97	2.97	2.95	2.96	2.95	2.97
Al	1.04	1.05	1.05	1.05	1.05	1.07	1.06	1.05	1.03
Fe	0	0.01	0	0	0	0	0	0	0
Ca	0.01	0.02	0.02	0.01	0.01	0.02	0.02	0.01	0.01
Na	0.13	0.11	0.14	0.13	0.11	0.12	0.11	0.14	0.13
K	0.84	0.87	0.85	0.82	0.85	0.82	0.83	0.88	0.86
An	1.43	1.64	1.57	1.07	1.33	1.79	2.31	0.86	0.93
Ab	12.77	11.15	13.85	13.97	11.09	12.41	11.50	13.61	13.36
Or	85.80	87.21	84.58	84.96	87.58	85.80	86.20	85.53	85.71

Table 4 EPMA compositions of the MI-hosting minerals – pyroxene

	P5XD	P5XA	P3XB
SiO_2	51.98	53.12	54.16
TiO_2	0.51	0.45	0.32
Al_2O_3	3.00	2.51	1.88
FeO	4.37	3.95	3.72
MnO	0.10	0.21	0.09
MgO	15.86	16.36	17.02
CaO	23.35	24.40	24.10
Na_2O	0.12	0.10	0.15
K_2O	0	0	0.02
Cr_2O_3	0.04	0.04	0.21
Si	1.92	1.92	1.94
Ti	0.01	0.01	0.01
Al IV	0.08	0.08	0.06
Al VI	0.05	0.03	0.02
Fe^{3+}	0.02	0.03	0.02
Fe^{2+}	0.12	0.09	0.09
Mn	0	0.01	0
Mg	0.87	0.88	0.91
Ca	0.92	0.95	0.93
Na	0.01	0.01	0.01
K	0	0	0
Cr	0	0	0.01
En	45.20	45.31	46.73
Fs	6.99	6.14	5.73

the MI and the hosting crystal (Fig. 3d, e). MI generally contain few large bubbles.
- Hourglass MI, with almond-like shapes. They generally have a very thin channel (few μm) propagating from the tip into the crystal. A deformed bubble generally occupies the tip of the MI, with few other bubbles scattered in the bulb.
- Thin films of glass filling fractures or swarms of lenticular, small (10–20 μm), devitrified, brown MI, are aligned along the fractures.

Leucite

Leucite is a very rare phenocryst phase. It is not a main crystallizing phase in the AD 79 magma, and it probably reaches the liquidus during the decompressional path accompanying the eruption (Rutherford 1996), so explaining its very high abundance in the groundmass (Cioni et al. 1995). The distribution of MI in leucite is strongly controlled by crystallographic planes, and they are generally arranged parallel to the crystal outlines. Acicular glass inclusions, abundant in leucite crystals from several other eruptions (Vaggelli et al. 1992; Marianelli 1994), are not very abundant in ejecta from this eruption. MI in leucite are brown to light coloured, and perfectly glassy. They have a rather high proportion of bubbles, generally positioned along the melt–crystal interface (Fig. 3g). Sometimes the bubbles are partly trapped in the crystal, suggesting post-entrapment growth of the leucite host. In this case, the large number of bubbles just at the melt–host interface could result from a post-entrapment oversaturation of the melt due to second boiling processes.

Pyroxene

As already remarked by Marianelli et al. (1995) and Cioni et al. (1995), pyroxene phenocrysts in the AD 79 products generally are diopsidic in composition. Fe-salitic pyroxenes occur either as rare microphenocrysts, mostly in white pumice, or as microlites, especially in the groundmass of the grey pumice. The studied MI-hosting crystals are unzoned diopside (Fs_{6-7}; Table 4) containing abundant MI which generally have a cryptocrystalline, dark appearance. After homogenization, MI become a light-brown colour, and are perfectly glassy (only one out of four has some square microlites of Ti-magnetite; Fig. 3f). They have faceted or lenticular shapes, and contain a large bubble and few small bubbles, or only an arrangement of tiny (few μm) bubbles all around the melt–crystal interface. In order to measure their volatile content, four homogenized MI were selected.

Composition of MI: major oxides

The comparison of MI composition with whole rock and groundmass glass analyses of samples from different

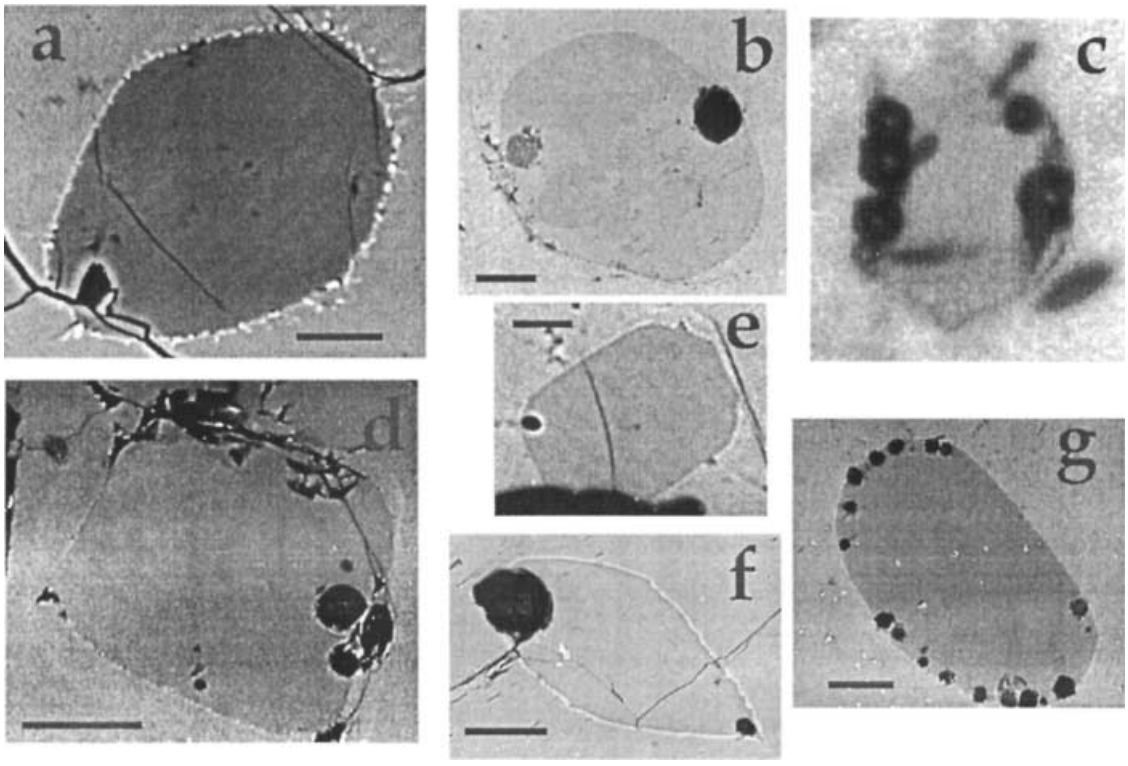

Fig. 3 SEM backscattered images (**a**, **b**, **d**, **e**, **f**, **g**) and microphoto (**c**) of some of the MI studied. **a** P5A, tiny shrinkage bubble; **b, c** R12E, bubble-rich MI; **d** T1E, frothy glass in the MI indicating post-trapping saturation and degassing; **e** T2E, tiny shrinkage bubble in a faceted MI; **f** P5Xa, very large bubble in an almond-shaped MI; **g** P2C1, characteristic appearance of MI in leucite, with a rim strongly enriched in bubbles deriving from second boiling. Some bubbles are clearly trapped in the host, suggesting post-trapping host crystallization

stratigraphic heights reveals several interesting features which need to be discussed in terms of the host mineral and of the post-trapping evolution of MI.

MI in sanidine

All MI in sanidine exhibit a phonolitic composition, slightly more evolved than white pumice (Fig. 4) as suggested by their lower CaO–FeO and higher SiO_2–K_2O contents. Depending on their host rock (white or grey pumice), MI in sanidine show different compositions, their K_2O/Na_2O ratio being higher ($\approx$2.3) in grey than in white ($\approx$1.8) pumice (Table 5).

MI in sanidine separated from white pumices (Wsd-MI) plot very close to the most evolved end member of the whole rock trend (Fig. 4). On the basis of mass balance calculations, the difference between the average composition of the Wsd-MI and the more evolved white pumices can be accounted for by the presence of 10–15 wt% phenocrysts (sanidine, clinopyroxene, amphibole and garnet) in the whole rock. This value is close to the modal estimate of phenocryst abundance in the white pumice (Table 4 in Cioni et al. 1995). The composition of Wsd-MI can therefore be assumed to be representative of the most evolved magma in the Pompeii chamber. Sample P1G (Table 5) shows an anomalously high content in K_2O and a corresponding low content of Na_2O, and I preferred not to consider it as a typical liquid composition. This conclusion is also supported by the shape of the MI, elongated parallel to a fracture in the crystal.

MI in sanidine from grey pumice (Gsd-MI) show a degree of evolution higher than Wsd-MI, especially reflected by SiO_2 content, which ranges between 58 and 59 wt% (56% in Wsd-MI), as well as CaO and FeO, which are lower than in Wsd-MI (Fig. 4 and Table 5). All these compositional differences can be interpreted in terms of the post-entrapment evolution of Gsd-MI, which can be derived from a salic magma with the composition of Wsd-MI by simple addition, through resorption, of sanidine (Fig. 5). Sigurdsson et al. (1990) and Cioni et al. (1995) related the occurrence of xenocrystic white sanidine in grey pumice to an important syn-eruptive mixing during the emission of the phonotephritic grey pumices. Sanidine resorption could have occurred during the re-heating of sanidine crystals (and of the hosted MI) due to this mixing event. On the basis of mass and heat balance, Cioni et al. (1995) estimated an equilibrium temperature of this mixing event of about 970 °C, well above the liquidus temperature of the phonolitic liquid trapped in MI, as measured from the T_{hom} of MI in sanidine (around 850 °C, Cioni et al. 1995) and calculated from MELTS (Ghiorso and Sack 1995) ($\approx$835 °C for 1.5 kbar, water saturation, $\Delta NNO = 0$). The extent of resorption varies from case to case, being in the range 30–50% by volume. This

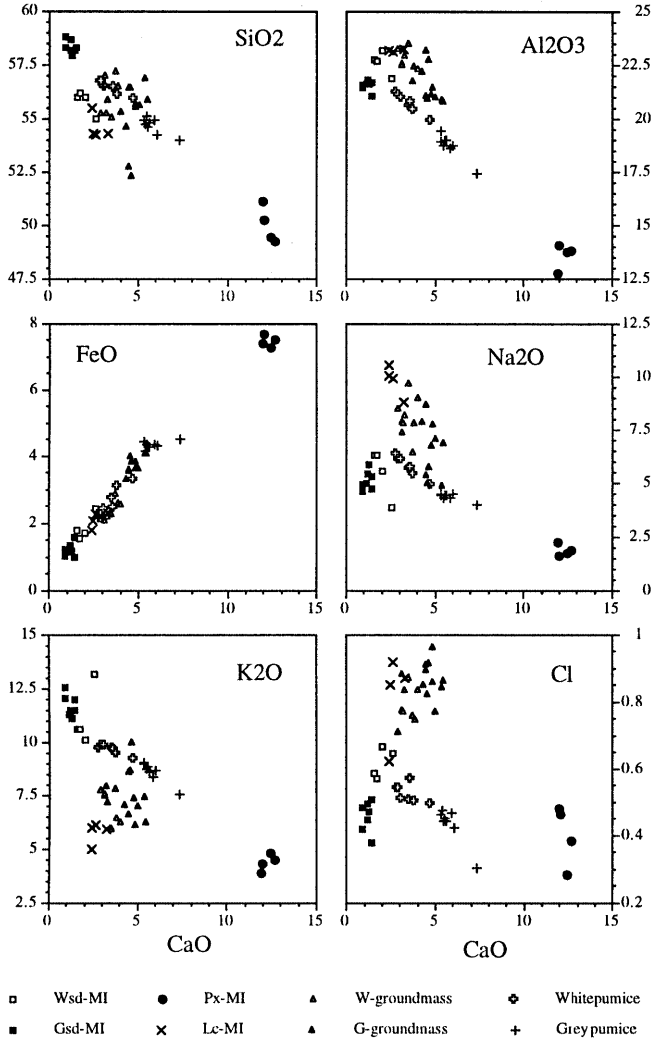

Fig. 4 Comparison between the compositional variation of the MI compared with the whole rock composition of the pumices and the groundmass glass of samples from different stratigraphic heights in the pumice fall deposit (data from Cioni et al. 1995)

implies, for an ideal, spherical, 100 μm inclusion, a resorption corona of 10–15 μm in thickness. The absence in Gsd-MI of any clear resorptional textural features should not be considered anomalous; Manley (1996), for example, studying MI in resorbed quartz from Badlands rhyolite lava flows (Idaho), found that some MI had enough time to mature back to negative crystal shapes after the resorptional event.

MI in leucite (Lc-MI)

The composition of Lc-MI is quite different from MI in sanidine, because of their higher Na_2O content and lower K_2O contents ($K_2O/Na_2O \approx 0.5$). Lc-MI plot close to the more evolved portion of the trend depicted by groundmass glasses (Fig. 4). This compositional trend is quite different from that shown by glasses hosted in sanidine, which align along the trend of the whole rocks.

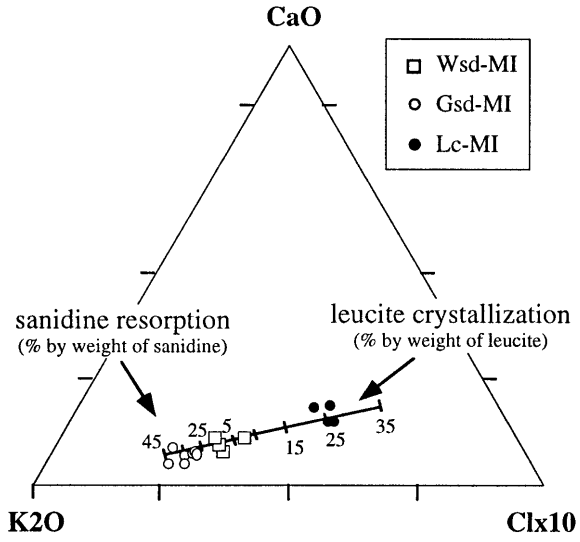

Fig. 5 The internal compositional variation recorded by the MI in the different host minerals, as evidenced by the ternary CaO–K_2O–Cl × 10 diagram

The very unusual composition of leucite-hosted MI can be interpreted as the result of a complex crystallization history. Clear textural indications of post-entrapment growth of the host on the inclusion walls are shown by the large number of bubbles arranged along the border of the MI, which are sometimes partially trapped in the crystal (Fig. 3g). The post-entrapment crystallization was at least 20–25% by volume. The different composition of MI in leucite and MI in sanidine can be related to crystallization of the leucite host on the inclusion walls. The stability field of leucite was tested using MELTS starting from the mean whole rock composition of white pumice (salic end member of Cioni et al. 1995) and of Wsd-MI, at pressures of 150–200 Mpa, temperatures of 850–900 °C, and fO_2 $\Delta NNO = 0$ as suggested by Rutherford (1996). The results indicate that leucite appears on the liquidus at 160–170 Mpa and 860–870 °C. Two different cases can be assumed:

- Leucite and sanidine were co-crystallizing phases, implying that the original Lc-MI composition was the same as Wsd-MI. If this is the case, mass balance calculations suggest that the present composition of Lc-MI resulted from the crystallization of 35–40 wt% of leucite.
- Leucite crystallized from a residual phonolitic melt, evolved through groundmass crystallization during syn-eruptive depressurization of magma. Starting from the composition of a leucite-bearing liquid calculated with MELTS in a quasi-isothermal decompression run (assumed to simulate magma ascent during eruption), MI composition in leucite must still be related to a certain (25–35 vol%), even if smaller, amount of crystallization of the host mineral.

I favour the second possibility, in agreement with the suggestions of Rutherford (1996), on the basis of some

Table 5 Composition of the MI studied. Major oxides, Ba, Sr, Cl and S from EMPA, and H_2O and CO_2 from FTIR analyses. The vol% occupied by the bubbles in the MI was based on volume estimations of measured bubbles and MI. H_2O data are calculated from the 3500 cm^{-1} absorption band. H_2O values marked with an *asterisk* are calculated from the sum of the concentrations of molecular water and hydroxyl as derived from the 5200 and 4500 cm^{-1} absorption bands. *bdl* Below detection limit; *nd* not detected

	Lc-MI				Wsd-MI				Gsd-MI							Px-MI			
	P5A	P1L	P2C1/1	P2C1/2	P1G	P2B	R12E	R12D	P4d	T1A	T2E	T2D	P5F1	T1 E	T2F	P5XA	P3XB	P5XD1	P5XD2
SiO_2	55.51	54.29	54.25	54.27	54.96	55.96	55.97	56.18	58.19	57.92	58.28	58.15	58.80	58.29	58.66	49.43	51.09	49.24	50.26
TiO_2	0.16	0.26	0.17	0.18	0.17	0.15	0.17	0.20	0.07	0.08	0.12	0.08	0.04	0.07	0.10	1.16	0.97	1.10	1.10
Al_2O_3	23.17	23.24	23.07	23.14	21.85	22.75	23.15	22.69	21.77	21.59	21.06	21.69	21.51	21.39	21.58	13.75	12.73	13.76	14.02
Cr_2O_3	bdl	bdl	bdl	bdl	bdl	bdl	bdl	bdl	bdl	bdl	bdl	bdl	bdl	bdl	bdl	0.02	0.05	0.01	0.01
FeO	1.78	2.31	2.25	2.06	2.43	1.78	1.72	1.56	1.15	1.19	1.57	0.98	1.03	1.21	1.33	7.27	7.37	7.50	7.68
MnO	0.14	0.13	0.12	0.18	0.19	0.18	0.13	0.14	0.07	0.09	0.09	0.08	0.07	0.12	0.06	0.14	0.17	0.14	0.17
MgO	0.06	0.12	0.05	0.05	0.21	0.21	0.02	0.12	0.02	0.06	0.04	0.02	0.02	0.04	0.05	7.56	7.81	6.93	6.52
CaO	2.40	3.26	2.62	2.42	2.57	1.58	2.03	1.73	1.20	1.25	1.44	1.43	0.91	0.89	1.16	12.43	11.95	12.64	12.02
Na_2O	10.55	8.75	9.93	10.01	3.82	6.26	5.50	6.31	5.39	5.85	4.73	5.28	4.89	4.62	4.98	1.72	2.21	1.83	1.61
K_2O	4.95	5.91	6.08	5.94	13.17	10.56	10.11	10.61	11.45	11.10	11.95	11.45	12.02	12.51	11.29	4.81	3.87	4.44	4.27
P_2O_5	bdl	bdl	bdl	bdl	bdl	bdl	bdl	bdl	bdl	bdl	bdl	bdl	bdl	bdl	bdl	0.77	0.60	1.11	0.96
Sr ppm	704	305	338	676	nd	nd	120	nd	148	209	149	592	bdl	bdl	bdl	695	1046	888	668
Ba ppm	bdl	bdl	bdl	223	nd	nd	63	nd	bdl	159	127	94	bdl	188	bdl	1152	1757	1412	1694
F	5500	7500	4800	7100	nd	nd	bdl	nd	bdl	3400	bdl	3400	bdl	3800	2600	bdl	bdl	3400	2600
SO_3	bdl	bdl	bdl	240	nd	nd	bdl	nd	bdl	bdl	bdl	bdl	bdl	bdl	bdl	840	1110	1260	1620
Cl	6240	8710	9180	8490	6470	5870	6650	5700	4450	4710	5060	3780	4810	4190	4960	2830	4800	3820	4620
H_2O tot	0.66	2.25	1.08	1.35	6.40*	nd	6.00*	3.21	3.97	6.49*	4.54	3.62	4.76	nd	4.95	2.00	3.38	3.01	3.04
CO_2 ppm	bdl	bdl	500	500	bdl	nd	bdl	bdl	bdl	bdl	bdl	bdl	bdl	nd	bdl	647	nd	1450	1450
% vesicles	1.60		3.00	1.00			6.00		1.50	1.50	1.00		11.00		10.00	6.50	17.00	0.00	0.00
Alk. ratio	0.47	0.68	0.61	0.59	3.44	1.69	1.84	1.68	2.13	1.90	2.53	2.17	2.46	2.71	2.27	2.80	1.75	2.43	2.66

Table 6 Concentrations of the different water and carbon species from FTIR analyses. The asterisks mark those MI where the 3500 cm^{-1} absorption peak was out of the detector scale

Sample	Type	Thickness [μm (± 1)]	Total H_2O				Molecula H_2O				Hydroxyl		CO_2	$AsCO_3^{2-}$
			3500 cm^{-1}	±	4500 + 5200 cm^{-1}	±	1630 cm^{-1}	±	5200 cm^{-1}	±	4500 cm^{-1}	±		±
PSA	Lc-MI	64	0.66	0.01	0.69	0.10	–	–	0.22	0.12	0.47	0.02	–	–
P1L	Lc-MI	25	2.25	0.63	2.59	–	–	–	1.27	–	1.32	–	–	–
P2Cl/1	Lc-MI	40	1.08	0.00	0.89	0.04	0.31	0.07	0.36	0.06	0.54	0.01	–	–
P2Cl/2	Lc-MI	40	1.35	0.03	1.04	0.12	0.38	0.03	0.40	0.03	0.64	0.10	–	–
P3A	Wsd-MI	27	5.20	0.42	4.65	0.51	–	–	3.25	0.24	1.40	0.29	–	–
P1G	Wsd-MI	46	*	–	6.40	0.18	–	–	4.80	0.47	1.60	0.29	–	–
R12E	Wsd-MI	67	*	–	6.00	0.44	4.37	0.69	4.68	0.34	1.32	0.11	–	–
R12D	Wsd-MI	23	3.21	–	3.46	–	–	–	2.41	–	1.05	–	–	–
P4D	GsD-MI	24	3.97	0.32	3.74	0.36	2.77	0.30	2.66	0.38	1.08	0.11	–	–
T1A	GsD-MI	18	*	–	6.49	0.05	4.48	0.32	4.44	0.02	2.05	0.03	–	–
T2E	GsD-MI	49	4.54	0.42	4.67	0.46	2.91	0.08	3.14	0.48	1.53	0.16	–	–
T2D	GsD-MI	49	3.62	0.03	3.83	0.05	2.47	0.04	2.35	0.07	1.48	0.01	–	–
P5F1	GsD-MI	28	4.76	0.22	4.80	0.09	3.67	0.24	3.73	0.07	1.07	0.14	–	–
T2F	GsD-MI	17	4.95	0.12	4.79	0.20	3.33	0.27	3.54	0.48	1.54	0.36	–	–
P5XA	Px-MI	24	2.00	0.14	2.65	0.16	0.72	0.04	1.51	0.18	1.12	0.02	647	96
P3XB	Px-MI	23	3.38	0.20	–	–	2.40	0.24	–	–	–	–	bdl	–
P5XD1	Px-MI	28	3.01	0.03	3.39	0.13	1.43	0.05	1.81	0.23	1.58	0.11	1489	167
P5XD2	Px-MI	28	3.04	0.04	3.64	0.55	1.53	0.03	2.06	0.35	1.58	0.21	1453	115

decompression experiments on the AD 79 phonolitic magma, and in accordance with the lesser degree of crystallization of the host on the inclusion walls, closer to the textural estimates. The very small number of leucite phenocrysts also support their very late crystallization.

MI in pyroxene (Px-MI)

After homogenization, Px-MI show a tephritic composition characterized by both high alkali content and high K_2O/Na_2O ratio. Compositions do not differ from those described in detail by Marianelli et al. (1995), and I mainly refer to that paper for further consideration.

Volatiles

Water and chlorine are the most interesting volatile phases in describing the pre-eruptive state of the AD 79 magma. CO_2 and S are always below the detection limit in phonolitic MI (Wsd-MI, Gsd-MI, Lc-MI), while CO_2 (dissolved as CO_3^{2-}) occurs at a high concentration only in some Px-MI. No clear relationship exists between volatile content and bubble volume in MI (Table 5). A correction for gas partitioned in the bubble was calculated (as in Anderson et al. 1989). However, the general absence of detectable CO_2 concentrations in the MI, and their low trapping pressure, reflect in a negligible gas partition to the bubble(s) of the MI.

Water in MI in sanidine and leucite

Total water content in MI in sanidine range from 3.5 to 6.5 wt% (Tables 5 and 6). Water content variability is often observed when analysing MI (Johnson et al. 1994). Possible causes lie in partial leakage of the inclusions during magma rise to the surface, and in post-entrapment crystallization of the host. The value which best approximates the pre-eruptive water content must be searched for on a one-by-one approach of the different measurements, based on the textural features and compositions of the MI. Based on these considerations, the best representatives for the pre-eruptive volatile content of the AD 79 magma are probably the Wsd-MI with the highest water concentrations, for which the resorptional effect of sanidine is less probable (P1G, R12 E, corresponding to 6–6.4 wt% total water; Tables 5 and 6). P1G, however, remains suspect due to its composition.

The other two Wsd-MI (P3 A, R12D) show quite clear evidence of syn-eruptive leakage, such as host fractures reaching the inclusions, which show highly vesicular, frothy glass very close to the contact with the fractures.

Gsd-MI have a water content ranging from 3.6 to 4.9 wt% (Tables 5 and 6). Only one MI (from a sample just at the base of the grey pumice fall layer) shows a very high water content (6.49 wt%; T1A; Table 5), similar to that measured in Wsd-MI. The generally lower water content shown by Gsd-MI with respect to Wsd-MI is in agreement with the sanidine resorption process undergone by Gsd-MI starting from compositions (and volatile contents) similar to that of Wsd-MI, and suggested on the basis of compositional features and mass balance calculations.

MI in leucite are generally extensively degassed. When corrected for the post-entrapment crystallization of the host, the very low water contents of MI (ranging from 0.6 to 2.2 wt%; Table 5) are additionally reduced by about 30%. This means that the composition of MI were evolving up to very low pressures (between 5 and a maximum of 34 MPa, according to the power law fit to solubility data given in Carroll and Blank 1997). In a general sense, leucite proved to be a bad "container" for MI. This was already noted by Marianelli et al. (1995), referring to MI homogenization. This can be related to the cooling history of leucite, which follows a second-order phase transformation from cubic to tetragonal symmetry with a continuous shrinkage of cell parameters with decreasing temperature. The main difference of such a transformation with respect to the famous quartz α–β inversion consists of a larger cell volume decrease (up to 6%) which does not occur discontinuously at a fixed temperature, but spans a very large T interval, starting from around 600 °C (Henderson 1984). The main effect of this behaviour is a continuous and increasing overpressure on the MI, even above the glass transition temperature appropriate for these compositions, going in the opposite sense to the relative contractional effect of the melt–crystal system (Tait 1992). The result is that MI tend to be cracked, with subsequent volatile leakage. The very low water contents indicate, however, that the system reached its glass transition (quenching) at a very shallow level.

Water speciation data

Data on the speciation of water in MI reflect the theoretical trend for speciation in glasses of Silver et al. (1990), with a regular increase of molecular water with increasing total water content, and an asymptotic increase of hydroxyl up to a maximum value of around 1.5 wt% (Fig. 6). Water speciation data in phonolitic MI fit very closely the experimental results obtained by Carroll and Blank (1997) on Na-phonolites (Fig. 6). The relative abundance of hydroxyl and molecular water depends on the quenching rate and can be envisaged as an indication of the temperature of relaxation of the system (Dingwell and Webb 1990; Ihinger 1991). With this assumption these data can be used as effective "geospeedometers" (Zhang 1994; Zhang et al. 1997).

Water speciation shows some small differences between samples from proximal and distal sites. MI from

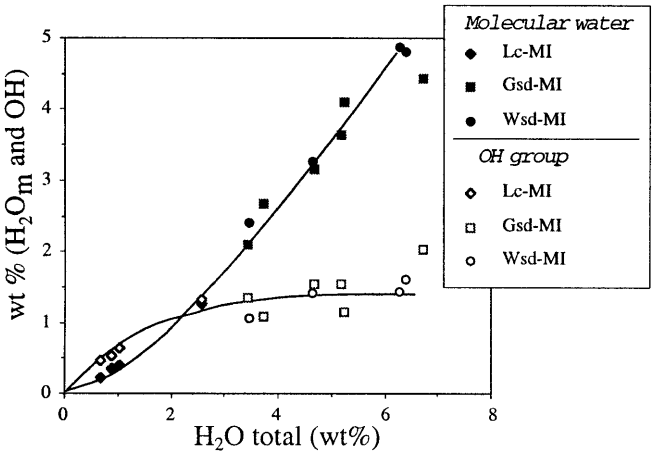

Fig. 6 Molecular water and hydroxyl concentrations in the MI vs. their total water content. The data fit very well the experimental relationship (*solid lines*) found by Carroll and Blank (1997)

samples of the distal fallout (Tricino site) have a generally higher OH content. This results in generally higher values of the apparent equilibrium constant of the homogeneous interchange reaction $H_2O^m_{mol} + O^m \rightarrow 2OH^m$ for similar total water contents (Fig. 7). If so few data can be interpreted in terms of cooling rates, we suggest that the higher Q', and consequently cooling rates, of samples from the more distal sites are related to a more efficient thermal coupling of clasts and air in the umbrella region of the Plinian column with respect to pumices released in the proximal sites from the margins of the column and settling with a higher accumulation rate (Thomas and Sparks 1994). An additional contributing factor in reducing the cooling rate in the proximal products could also be related to the thicker accumulation of hot deposits, essentially due to the presence of thick pyroclastic flow deposits.

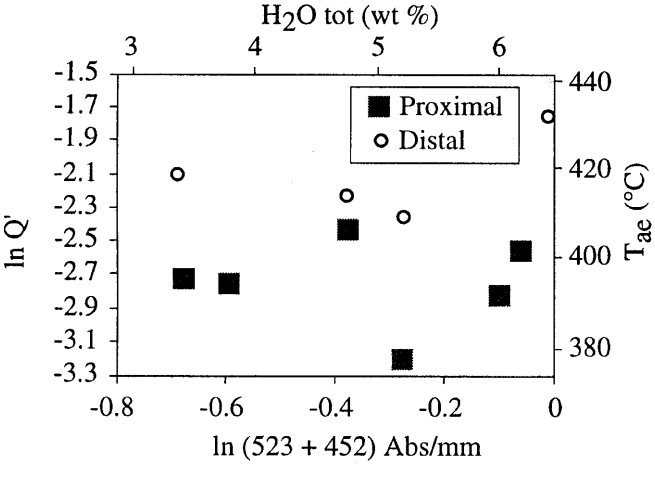

Fig 7. Diagram of total water vs. the equilibrium constant of the interchange reaction $H_2O^m_{mol} + O^m \rightarrow 2OH^m$ using $\ln(Abs_{5230} + Abs_{4520})$ as proxy for total water content and $\ln[(Abs_{4520})^2/Abs_{5230}]$ as proxy for the equilibrium constant (as suggested by Zhang et al. 1997; Abs_{5230} and Abs_{4520} are the absorbancies for mm sample thickness)

On the other hand, we can estimate that glass transition for the most distal glasses occurred at around 400 and 430 °C, assuming the validity of the relation given in Zhang et al. (1997) for rhyolitic liquids.

Water and CO_2 in pyroxene

Determination of water and CO_2 content of tephritic melts was performed on four MI from three clinopyroxene crystals. They give water contents ranging from 2 to 3.4 wt% (Tables 5 and 6), the lower value being associated with a MI showing a very large bubble (Table 5 and Fig. 3f). All spectra show a very distinct absorption peak around 1630 cm^{-1}, in three samples somewhat disturbed on the high frequency side by the superposition of a very clear CO_3^{2-} absorption doublet. Best guesses of total water content are probably represented by the results based on the absorption value of 3530 cm^{-1}. Although the molar absorptivity for this peak is in fact less sensitive to composition than those for the other peaks, the data on water speciation of Table 6 must be considered with caution, because of the absence of specific values of molar absorptivity for tephritic compositions. Water content as determined by FTIR is on average higher than water content determined by SIMS analyses on corresponding samples, which range from 1.3 to 2.3 wt% (Table 7 in Cioni et al. 1995).

CO_2 is present as carbonate complexes in all but one (P5XA) sample. A CO_2 content of 1450 ppm is given by the two MI in P5XD pyroxene, while 650 ppm were found in P5XA, associated with the lowest water concentration and a large bubble (accounting for 6.5% of the whole MI volume). The minimum saturation pressure for the MI was obtained using the calculation procedure of Dixon and Stolper (1995), modified to account for melt composition according to the suggestions of Dixon (1997). For P5XA, the equilibrium composition of vapour was used to estimate the minimum CO_2 content of the bubble, assuming closed-system degassing and the vapour mixture density at the saturation pressure. Given these assumptions, the bubble gives a very large contribution to the total volatile content of the liquid, raising the water content by around 20% and suggesting a very high CO_2 content, of several thousand parts per million.

Chlorine, fluorine and sulphur

Chlorine is very abundant in all the phonolitic MI, ranging from 5700 to 6700 ppm in Wsd-MI in sanidine, from 3800 to 5100 in Gsd-MI, and from 6200 up to 9200 ppm in MI in leucite. Such a high content is very close to that measured in some peralkaline magmas (Lowenstern 1994b). Metrich and Rutherford (1992) measured a saturation value of 6270 ppm for the Vesuvius AD 79 phonolitic magma at 1 kbar, and a very

faint dependence of Cl solubility on pressure. This value coincides with the mean value for Wsd-MI. The low Cl content of Gsd-MI is in agreement with the resorption process of sanidine proposed to explain the compositional differences. Groundmasses of white and grey pumices have a very high chlorine content, in the range 8000–8600 ppm, closer to the content of MI in leucite. Chlorine content is high also in tephritic MI in pyroxene, with an average of 4000 ppm. Such a content is greater than that commonly reported for mafic magmas (Carroll and Webster 1994), and it is at the lower end of the range found by Marianelli et al. (1995) in similar compositions.

Webster (1997) described a linear relation between chlorine solubility and the molar (Al + Na + Ca + Mg)/Si ratio of the melt. Such a variation is also shown by the chlorine in MI of the present paper, with MI in leucite having practically the same ANCM/S ratio as the groundmasses (Fig. 8).

Fluorine determinations in the studied samples are not very reliable due to the analytical technique. However, fluorine seems to be particularly enriched in MI in leucite with respect to MI in sanidine (Table 5). Such behaviour suggests an important F retention during the crystallization process, in agreement with the coupling between F and Cl solubilities observed by Webster (1997) and with the strong enrichment in Cl of such MI.

Sulphur is present in detectable concentrations only in MI in pyroxenes, where it shows concentrations between 840 and 1600 ppm. Sulphur in phonolitic MI (both in sanidine and leucite) and pumice groundmasses was always below the detection limit.

Discussion

The composition and volatile content of phonolitic MI (in sanidine and leucite) can be used to discuss the pre-eruptive state of the chamber and to assess the amount and modalities of the syn-eruptive release of gaseous species. Information on the pre-eruption state of the lower, mafic (tephri-phonolitic) portion of the chamber is precluded by the absence of a sound mineral assemblage in equilibrium with this portion of the magma body (Cioni et al. 1995). However, some inferences on this portion can be drawn from the data on MI in diopsidic pyroxenes, which represent the liquid closest to the composition of the magma batches feeding the chamber (Marianelli et al. 1995).

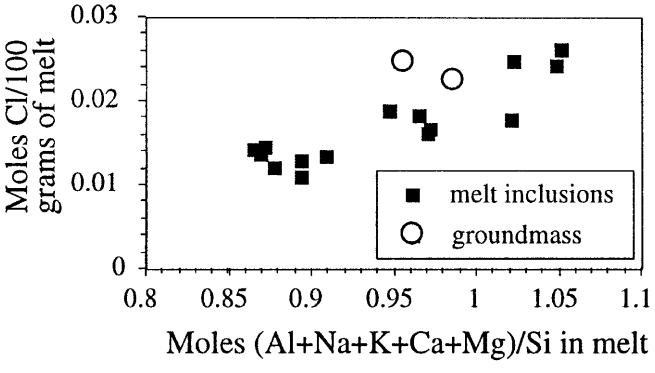

Fig. 8 ANKCM/S vs. Cl for MI and groundmass glass of both white and grey pumices

Pre-eruptive volatile composition

Phonolitic MI in sanidine formed during crystallization in the upper portion of the AD 79 magma chamber. They show a relatively wide variability, which can be reduced when accounting for the post-entrapment evolution of the MI.

The presence of a separated fluid phase in the magma chamber prior to the eruption is indicated by the presence of amphibole in the mineral assemblage. However, the absence of fluid inclusions in minerals, and the absence of evidence of multiphase (liquid + vapour) trapping, suggest that this fluid phase was probably not very abundant. The frequent presence of several spherical bubbles in the MI (Fig. 3c) can be explained by the reaching of supersaturation during isochoric cooling of the MI (Lowenstern 1994a) or by a second boiling process due to host crystallization.

The very good agreement of water speciation data on these K-phonolitic MI with the experimental data on Na-phonolitic glasses presented by Carroll and Blank (1997; Fig. 6) allow us to use their results confidently for water solubility. Using their empirical relation for the pressure dependence of H_2O solubility ($H_2O_{wt\%} = 0.0329P_{bar}^{0.7238}$), the minimum (saturation) pressure of the phonolitic magma in the upper portion of the chamber (represented by the Wsd-MI with the most reliable highest water content, 6.0 wt%), is about 150 MPa, corresponding to a 4–6 km depth range. A similar conclusion was also reached by Barberi and Leoni (1980) and Barberi et al. (1981), on the basis of the indications given by the mineral paragenesis of thermometamorphic ejecta and pumice petrology. On the other hand, saturation pressure seems to be a good approximation to pre-eruption pressure, as suggested by the experimental work of Rutherford (1996) where water saturation ($X_{H_2O} = 1$) is indicated as the most reliable condition to stabilize the equilibrium mineralogical assemblage of white pumice. This contrasts with the conclusions of Signorelli et al. (1999) on the products of another Plinian eruption of Vesuvius (the Avellino Pumice), who suggest the presence of a CO_2 rich fluid phase ($X_{H_2O} = 0.4$) during magma chamber evolution.

Cioni et al. (1995), using caldera area and erupted magma volume, inferred an ellipsoidal magma chamber with a vertical extent not greater than 1 km. This would imply a magmastatic pressure excess at the bottom of the magma chamber not greater than 20–25 MPa, ruling out the possibility of an important gradient in water solubility (and content) for the phonolitic magma, occupying the upper half of the chamber.

Inferences on the modalities of magma chamber feeding and evolution

The tephritic MI in diopside give some constraints to the maximum water and CO_2 contents of the mafic magma batches feeding the chamber. According to the water–CO_2 solubility models presented by Dixon and Stolper (1995) and Dixon (1997) for basalts with different alkalinity, MI with the highest volatile content (P5XD1 and P5XD2, Table 5) give a minimum trapping pressure of around 350 MPa. On the other hand, one MI (P3XB) containing no CO_2 and high H_2O gives a minimum pressure of around 140 MPa, close to that estimated for the phonolitic portion of the magma chamber. The variability in the volatile content of these MI suggests that diopside could have formed both during ascent of magma batches towards the shallow reservoir, and during its mixing with the resident magma (Marianelli et al. 1995, 1999). The very few data presented here do not allow us to make inferences on the degassing paths followed by the tephritic melts feeding the chamber. However, the very similar vapour phase composition at saturation for H_2O and CO_2-bearing MI equilibrated to high pressure (P3XD) and low pressure (P5XA; respectively $X^{vap}_{H_2O}$ of 0.38 and 0.35) would suggest a closed system degassing (Dixon and Stolper 1995) of the tephritic batches entering the chamber. Following this decompressional path, the total loss of CO_2 shown by P3XB MI (Table 6) should have occurred after the tephritic batches entered the chamber. This explains the absence of dissolved CO_2 in the upper phonolitic magma body, which grows from the differentiation of the lower tephri-phonolitic magma (Cioni et al. 1995). Even with the assumption of closed-system degassing, CO_2 exsolution from the magma towards a fluid with a mean $X^{vap}_{H_2O}$ of 0.36 implies that the mafic batches entering the chamber were only slightly vesicular (not more than 1–2 vol%), so probably not greatly affecting the mixing processes in the lower portion of the chamber.

The large difference between water content of tephrite and phonolite suggests that during chamber evolution water preferentially accumulated in the magma. In this case, if some of the CO_2 was lost after the mafic batches entered the chamber, this degassing should have occurred in open-system-like conditions, allowing the preferential loss of CO_2 with respect to H_2O (Dixon 1995).

The partial crystallization of magma batches entering the chamber while reaching the thermal equilibrium with the resident magma can be traced semi-quantitatively using MELTS. Cooling of the feeding magma to the estimated temperature of the resident magma (around 1050 °C) leads to a maximum crystallization lower than 35% by weight. Even in such an extreme case, water content does not reach the solubility limit (estimated using the Burnham model), thus allowing water to concentrate in the lower part of the magma body.

Besides degassing of CO_2, the evolution path which produced the phonolitic portion of the magma chamber surely also implied sulphur loss (the sulphur content is below the detection limit in phonolitic MI). Sulphur solubility is strongly controlled by the redox conditions of the melt and by its composition (especially iron content; Carroll and Webster 1994). Mixing of magmas with different compositions and oxygen fugacities can also dramatically affect S behaviour (Kress 1997). All these facts variably influenced the evolution of the AD 79 magma, and in the absence of any specific experimental data on S solubility in tephritic and phonolitic magmas, we are at present not able to specify which process dominantly affected sulphur behaviour.

The conclusion is that magma chamber evolution probably occurred under fluxing of CO_2 and sulphur from the lower portion of the magma body, together with a contemporaneous accumulation in magma of water, chlorine and fluorine.

Syn-eruptive degassing and volatile contribution to the atmosphere

The measurement of the volatile content of the residual glasses by FTIR spectroscopy was not possible due to the highly crystalline nature of pumice matrix glasses. Therefore, water dissolved in the residual melt has been roughly assessed from pumice vesicularity and initial water content (Gardner et al. 1996). The white pumice vesicularity ranges from 70 to 80% by volume (gas/liquid volume ratio in the range 2.5–5). With the assumption that pumice vesicularity did not evolve after fragmentation or through development of foam permeability, these values suggest that the water not exsolved from the liquid varies from 1.1 to 1.6% by weight. In discussing syn-eruptive degassing, the minimum value of the water exsolved during the final magma ascent can therefore be assumed to vary between 4.9 and 5.4 wt%. It is important to note that water remaining in the melt is very close to the concentration measured in MI in leucite (Table 5), which was interpreted as crystallized during magma ascent to the surface. If such an assumption is valid, this means that the strong crystallization of leucite occurred just around the fragmentation level, in coincidence with the maximum pressure gradient (Wilson et al. 1980).

The behaviour of chlorine during eruption can be inferred from chlorine content of residual matrix glasses and initial content of the melt (as derived by Wsd-MI). The extensive crystallization of leucite in the groundmass of white pumices (about 40% on the basis of mass balance calculations) was accompanied by a slightly lower Cl enrichment (around 30%). Based on the volatile content of phonolitic MI and white pumice matrix glasses, the estimated Cl loss during decompressional groundmass crystallization was around 400 ppm, and the fluid/melt partition coefficient of chlorine (D_{Cl}) was around 2–3. This value is very low if compared to those calculated for granitic compositions (Shinohara et al. 1989; Webster 1992), and is even smaller than those

calculated by Barclay et al. (1996) for the peralkaline magmas of Mayor Island. Possible explanations for such behaviour were discussed in Barclay et al. (1996) and, with the assumption of second-order P–T dependence of Cl solubility, may be reduced to the following two points:

1. Differential diffusion rates of water and chlorine during rapid decompression.
2. Compositional dependence of chlorine solubility.

Our data seem to suggest a strong effect of the second mechanism. Water degassing was accomplished by extensive crystallization and strong chlorine enrichment. Chlorine was only partially degassed during this process and the chlorine content of residual glasses is clearly dependent on melt composition (Fig. 8). Widespread leucite crystallization shifts the melt toward a higher ANKCM/S molar ratio (ANKCM = sum of the molar fractions in the melt of Al_2O_3, Na_2O, K_2O, CaO, MgO; S = molar fraction in the melt of SiO_2), and the linear arrangement shown by the data, together with the partial loss of chlorine during degassing, suggests that chlorine reached saturation even though its solubility in the residual glasses was increasingly higher.

In this situation, chlorine contribution to the atmosphere appears to have been quite low, and can be calculated from petrologic and volcanological data (Gerlach et al. 1994) at no more than 1 Mt of Cl for a maximum of 100 Mt of water. The detection limit of our analyses (around 200 ppm S) prevented calculation of a reliable estimate of S release. It was probably lower than Cl release, because S values measured on whole samples (by XRF) are of the same order of magnitude as those on MI (Table 1 in Cioni et al. 1995), thus supporting the idea that an important loss of S must have preceded the eruption.

Conclusions

A model of the AD 79 magma chamber was presented by Cioni et al. (1995), based on geochemical, MI and isotopic data, as well as on the sequence of magma extraction. The model involves a two-fold magma chamber, where the magmatic differentiation which forms the upper, evolved, phonolitic layer is mainly related to the repeated evolution and overturning of an interface volume where the rate of magma evolution is greater than in the lower, less evolved portion of the chamber. The thermal life of the chamber is guaranteed by the periodic arrival of deep, mafic magma batches which partially crystallize and mix with the magma residing in the lower portion of the chamber.

The different stages of crystallization are marked by different mineral phases. Data on volatile contents in MI from these crystals contribute to our understanding of the processes of volatile accumulation and degassing in the different portions of the magma chamber (Fig. 9).

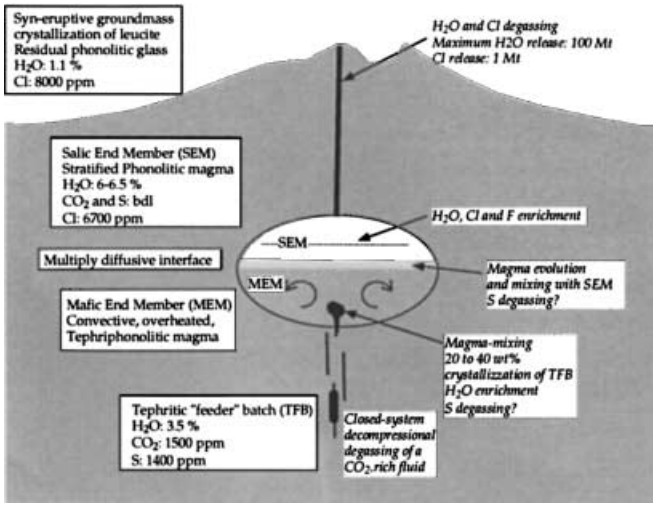

Fig. 9 Sketch of the AD 79 magma chamber (modified after Cioni et al. 1995), showing the inferred stages of evolution of the volatile components (see text for further explanation)

1. Magma batches feeding the chamber can be investigated from MI in diopside (Marianelli et al. 1995). Infrared measurements give maximum concentrations of 3% H_2O and 1500 ppm CO_2, corresponding to minimum trapping pressures of around 300 MPa. Partial (closed-system) degassing occurs during the decompressional path to the magma chamber. CO_2 was probably completely degassed after the batches entered the magma chamber.

2. No information is available on the volatile content of the lower portion of the magma chamber (mafic end member, Fig. 9), due to the lack of a certain mineral assemblage in equilibrium with this composition.

3. The evolution of the lower magma body (mafic end member) to feed the salic end member sited in the upper portion of the chamber occurs in a restricted interface volume (Cioni et al. 1995). Crystallization can lead to a rapid, composition-related, decrease of S solubility in the residual liquid. Moreover, the periodic mixing between this evolving magma and the upper phonolitic liquid can shift fO_2 conditions of the system to a situation of minimum S solubility.

4. Water, chlorine and fluorine strongly concentrate in the upper portion of the chamber, where they can reach the solubility limit. Strong decompressional degassing accompanied the eruption, as testified by pumice groundmasses and MI in leucite, which undergoes extensive crystallization during this stage. Water speciation recorded in MI seems to be related to post-depositional cooling rates.

5. Chlorine behaviour is strongly influenced by magma composition. The high residual content of Cl in pumice groundmasses can be explained by a syn-eruptive shift of the composition of the residual liquid to a higher Cl solubility. This is reflected in a very low Cl partition coefficient in the fluid phase. A general conclusion can be that phonolitic Plinian eruptions at

Vesuvius did not have a great Cl release to the atmosphere, so did not contribute to raising the stratospheric HCl background signal.

6. As a concluding remark, it is important to emphasize the relevance of MI studies in the volatile accumulation and degassing history of a magma chamber. The bimodal distribution of MI composition and volatile content in identical sanidine from pumice of different compositions must be related to host resorption during syn-eruptive mixing processes rather than to pre-eruption differences. These studies must therefore be associated with a detailed volcanological and geochemical study of the erupted products, in order to identify the different pre- and syn-eruptive processes which condition the composition of the magma.

Acknowledgements I am indebted to Ed Stolper and George Rossmann for having permitted access to the laboratories of the Geological and Planetary Sciences Division at Caltech, Pasadena (CA), and especially to Sally Newman for her training and assistance during sample preparation and FTIR measurements. I am grateful to Roberto Santacroce and Sally Newman for their thorough reviews of the manuscript, and to Jaquelin Dixon and Marie Johnson for their very kind comments. The work was funded by Gruppo Nazionale di Vulcanologia, National Council of Research, Italy.

References

Anderson AT Jr, Newman S, Williams SN, Druitt TH, Skirius C, Stolper E (1989) H_2O, CO_2, Cl and gas in Plinian and ash-flow Bishop rhyolite. Geology 17: 221–225

Barberi F, Leoni L (1980) Metamorphic carbonate ejecta from Vesuvius Plinian eruptions: evidence of the occurrence of shallow magma chambers. Bull Volcanol 43: 107–120

Barberi F, Bizouard H, Clocchiatti R, Metrich N, Santacroce R, Sbrana A (1981) The Somma–Vesuvius magma chamber: a petrological and volcanological approach. Bull Volcanol 44: 295–315

Barclay J, Carroll MR, Houghton BF, Wilson CJN (1996) Pre-eruptive volatile content and degassing history of an evolving peralkaline volcano. J Volcanol Geotherm Res 74: 75–87

Behrens H, Romano C, Nowak M, Holtz F, Dingwell DB (1996) Near-infrared spectroscopic determination of water species in glasses of the system $M_lSi_3O_8$ (M = Li, Na, K): an interlaboratory study. Chem Geol 128: 41–63

Blank JG, Brooker RA (1994) Experimental studies of carbon dioxide in silicate melts: solubility, speciation and stable carbon isotope behaviour. In: Carroll MR, Holloway JR (eds) Volatiles in magmas. MSA Rev Mineral vol 30, pp 157–186

Carroll MR, Blank JG (1997) The solubility of H_2O in phonolitic melts. Am Mineral 82: 549–556

Carroll MR, Webster JD (1994) Solubilities of sulfur, noble gases, nitrogen, chlorine and fluorine in magmas. In: Carroll MR, Holloway JR (eds) Volatiles in magmas. MSA Rev Mineral vol 30, pp 231–279

Church BN, Johnson WM (1980) Calculation of the refractive index of silicate glasses from chemical composition. Geol Soc Am Bull 91: 619–625

Cioni R, Marianelli P, Sbrana A (1992) Dynamics of the AD 79 eruption: stratigraphic, sedimentologic and geochemical data on the successions of the Somma–Vesuvius southern sector. Acta Vulcanol 2: 109–123

Cioni R, Civetta L, Marianelli P, Metrich N, Santacroce R, Sbrana A (1995) Compositional layering and syn-eruptive mixing of a periodically refilled shallow magma chamber: the AD 79 Plinian eruption of Vesuvius. J Petrol 36: 739–776

Dingwell DB, Webb SL (1990) Relaxation in silicate melts. Eur J Mineral 2: 427–449

Dixon JE (1997) Degassing of alkalic basalts Am Mineral 82: 368–378

Dixon JE, Pan V (1995) Determination of the molar absorptivity of dissolved carbonate in basanitic glasses. Am Mineral 80: 1339–1342

Dixon JE, Stolper E (1995) An experimental study of water and carbon dioxide solubilities in mid-ocean ridge basaltic liquids. Part II: Applications to degassing. J Petrol 36: 1633–1646

Dixon JE, Stolper E, Holloway JR (1995) An experimental study of water and carbon dioxide solubilities in mid-ocean ridge basaltic liquids. Part I: Calibration and solubility models. J Petrol 36: 1607–1631

Dobson PF, Epstein S, Stolper EM (1989) Hydrogen isotope fractionation between coexisting vapor and silicate glasses and melts at low pressure. Geochim Cosmochim Acta 53: 2723–2730

Gardner JE, Thomas RME, Jaupart C, Tait S (1996) Fragmentation of magma during Plinian volcanic eruptions. Bull Volcanol 58: 144–162

Gerlach TM, Westrich HR, Casadevall TJ, Finnegan DL (1994) Vapor saturation and accumulation in magmas of the 1989–1990 eruption of Redoubt volcano, Alaska. J Volcanol Geotherm Res 62: 317–337

Ghiorso MS, Sack RO (1995) Chemical mass transfer in magmatic processes. IV. A revised and internally consistent thermodynamic model for the interpolation and extrapolation of liquid–solid equilibria in magmatic systems at elevated temperatures and pressures. Contrib Mineral Petrol 119: 197–212

Henderson CMB (1984) Feldspathoid stabilities and phase inversions – a review. In: Brown WL (ed) Feldspars and feldspathoids. Reidel, Dordrecht, pp 471–499

Holloway JR, Blank JG (1994) Application of experimental results to C–O–H species in natural melts. In: Carroll MR, Holloway JR (eds) Volatiles in magmas. MSA Rev Mineral vol 30, pp 187–230

Ihinger PD (1991) An experimental study of the interaction of water with granitic melt. PhD Thesis, Calif Inst Tech

Ihinger PD, Hervig RL, McMillan PF (1994) Analytical methods for volatiles in glasses. In: Carroll MR, Holloway JR (eds) Volatiles in magmas. MSA Rev Mineral vol 30, pp 67–121

Jacobsson S (1997) Solubility of water and carbon dioxide in an icelandite at 1400 °C and 10 kilobars. Contrib Mineral Petrol 127: 129–135

Johnson MC, Anderson AT Jr, Rutherford MJ (1994) Pre-eruptive volatile contents of magmas. In: Carroll MR, Holloway JR (eds) Volatiles in magmas. MSA Rev Mineral vol 30, pp 281–330

Kress V (1997) Magma mixing as a source for Pinatubo sulphur. Nature 389: 591–593

Lowenstern JB (1994a) Applications of silicate-melt inclusions to the study of magmatic volatiles. In: Thompson JFH (ed) Magmas, fluids, and ore deposits. MAC Short Course Ser 23, pp 71–99

Lowenstern JB (1994b) Chlorine, fluid immiscibility, and degassing in peralkaline magmas from Pantelleria, Italy. Am Mineral 79: 353–369

Manley CR (1996) Morphology and maturation of melt inclusions in quartz phenocrysts from the Badlands rhyolite lava flow, southwestern Idaho. Am Mineral 81: 158–168

Marianelli P (1994) La camera magmatica del Vesuvio: processi petrogenetici e dinamica eruttiva. PhD Thesis, Università degli Studi di Pisa

Marianelli P, Metrich N, Santacroce R, Sbrana A (1995) Mafic magma batches at Vesuvius: a glass inclusion approach to the modalities of feeding stratovolcanoes. Contrib Mineral Petrol 120: 159–169

Marianelli P, Metrich N, Sbrana A (1999) Shallow and deep reservoirs involved in magma supply of the 1944 eruption of Vesuvius. Bull Volcanol 61: 48–63

Metrich N, Rutherford MJ (1992) Experimental study of chlorine behaviour in hydrous silicic melts. Contrib Mineral Petrol 56: 607–616

Mues-Schumacher U (1994) Chemical variations of the AD 79 pumice deposits of Vesuvius. Eur J Mineral 6: 387–395

Newman S, Stolper EM, Epstein S (1986) Measurement of water in rhyolitic glasses: calibration of an infrared spectroscopic technique. Am Mineral 71: 1527–1541

Papale P (1997) Modeling of the solubility of a one component H_2O or CO_2 fluid in silicate liquids. Contrib Mineral Petrol 126: 237–251

Romano C, Dingwell DB, Behrens H (1995) The temperature dependence of the speciation of water in $NaAlSi_3O_8$–$KAlSi_3O_8$ melts: an application of fictive temperatures derived from synthetic fluid-inclusions. Contrib Mineral Petrol 122: 1–10

Rutherford MJ (1996) Conditions in the pre-eruption 79 AD Vesuvius magmas: controls on magmatic and eruption processes. In: Vesuvius Decade Volcano. Workshop Handbook. IAVCEI–CEV, IAVCEI–CMVD, 17–22 September 1996 (Abstr)

Shinohara H, Iiyama JT, Matsuo S (1989) Partition of chlorine compounds between silicate melt and hydrothermal solutions: I. Partition of NaCl–KCl. Geochim Cosmochim Acta 53: 2617–2630

Signorelli S, Vaggelli G, Romano C (1999) Pre-eruptive volatile (H_2O, F, Cl and S) contents of phonolitic magmas feeding the 3550-year-old Avellino eruption from Vesuvius, Southern Italy. J Volcanol Geotherm Res 93: 237–256

Sigurdsson H, Carey S, Cornell W, Pescatore T (1985) The eruption of Vesuvius in 79 AD. Nat Geogr Res 1: 332–387

Sigurdsson H, Cornell W, Carey S (1990) Influence of magma withdrawal on compositional gradients during the AD 79 Vesuvius eruption. Nature 345: 519–521

Silver LA, Ihinger PD, Stolper E (1990) The influence of bulk composition on the speciation of water in silicate glasses. Contrib Mineral Petrol 104: 142–162

Sparks RSJ (1986) The dimensions and dynamics of volcanic eruption columns. Bull Volcanol 48: 3–15

Stolper E (1982) Water in silicate glasses: an infrared spectroscopic study. Contrib Mineral Petrol 81: 1–17

Tait S (1992) Selective preservation of melt inclusions in igneous phenocrysts. Am Mineral 77: 146–155

Thomas RME, Sparks RSJ (1994) Cooling of tephra during fallout from eruption columns. Bull Volcanol 54: 542–553

Vaggelli G, Belkin HE, De Vivo B, Trigila R (1992) Silicate-melt inclusions in recent Vesuvius lavas (A.D. 1631–1944): I. petrography and microthermometry. Eur J Mineral 4: 1113–1124

Webster JD (1992) Fluid–melt interactions involving Cl-rich granites: experimental study from 2 to 8 kbar. Geochim Cosmochim Acta 56: 659–678

Webster JD (1997) Chloride solubility in felsic melts and the role of chloride in magmatic degassing. J Petrol 38: 1793–1807

Wilson L, Sparks RSJ, Walker GPL (1980) Explosive volcanic eruptions – IV. The control of magma properties and conduit geometry on eruption column behaviour. Geophys J R Astron Soc 63: 117–148

Zhang Y (1994) Reaction kinetics, geospeedometry, and relaxation theory. Earth Planet Sci Lett 122: 373–391

Zhang Y, Jenkins J, Xu Z (1997) Kinetics of the reaction $H_2O + O \leftrightarrow 2OH$ in rhyolitic glasses upon cooling: geospeedometry and comparison with glass transition. Geochim Cosmochim Acta 61: 2167–2173